

High-Field, Quasi-Ballistic Transport in Short Carbon Nanotubes

Ali Javey,¹ Jing Guo,² Magnus Paulsson,² Qian Wang,¹ David Mann¹, Mark Lundstrom²
and Hongjie Dai¹

¹ Department of Chemistry and Laboratory for Advanced Materials, Stanford University,
Stanford, CA, 94305

² School of Electrical and Computer Engineering, Purdue University, West Lafayette, IN,
47907

Single walled carbon nanotubes with Pd ohmic contacts and lengths ranging from several microns down to 10 nm are investigated by electron transport experiments and theory. The mean free path (mfp) for acoustic phonon scattering is estimated to be $l_{\text{ap}} \sim 300$ nm, and that for optical phonon scattering is $l_{\text{op}} \sim 15$ nm. Transport through very short (~ 10 nm) nanotubes is free of significant acoustic and optical phonon scattering and thus ballistic and quasi-ballistic at the low and high bias voltage limits respectively. High currents of up to 70 μA can flow through a short nanotube. Possible mechanisms for the eventual electrical breakdown of short nanotubes at high fields are discussed. The results presented here have important implications to high performance nanotube transistors and interconnects.

Email: hdai@stanford.edu

Recent progress in ohmic contacts to single-walled carbon nanotubes (SWNTs) has facilitated the elucidation of the intrinsic electron transport properties of these novel materials and the advancement of high performance nanotube electronics.¹⁻⁶ With high quality as-grown chemical vapor deposition (CVD) materials and ohmic contact strategies, several groups have observed ballistic electron transport in metallic nanotubes,^{2,3} and more recently, in semiconducting SWNTs by Javey et al.⁵ The hallmark of ballistic transport in SWNTs is the conductance (G) of the samples reaching four quantum units $4e^2/h$ (resistance $R \sim 6.5 \text{ k}\Omega$) and the manifestation of phase coherent resonance at low temperatures.^{2,3,5,7} However, observations of ballistic transport in SWNTs have been mostly limited at the low bias voltage ($< 0.1 \text{ V}$) regime thus far. Yao et al. have shown that in the high bias ($> 0.16 \text{ V}$) regime, current saturation at the $25 \text{ }\mu\text{A}$ level occurs due to electron backscattering by optical or zone boundary phonon emissions.¹ Similar current saturation has been observed in ohmically contacted semiconducting SWNTs recently.⁵ These results hint that for SWNTs longer than the mfp of optical phonon scattering (l_{op} in the range of $10 - 100 \text{ nm}$ from Ref. 1), high bias electron transport is not truly ballistic.

Here, we investigate ohmically contacted metallic SWNTs with lengths systematically scaled from the micron scale down to 10 nm . Pd metal affords near ohmic contacts to these nanotubes with very high reproducibility,^{5,7} a key to this investigation. Theoretical analysis and fitting of experimental data reveal $l_{\text{ap}} \sim 300 \text{ nm}$ and $l_{\text{op}} \sim 15 \text{ nm}$. Consequences of these length scales include, first, for metallic SWNTs with length $L \ll l_{\text{ap}}$, the low bias conductance is essentially ballistic and nearly temperature independent. Second, for nanotubes with $L \sim 10 \text{ nm}$, the current carrying capability reaches up to 70

μA , well exceeding the highest ($25 \mu\text{A}$) reported previously. Short SWNTs are, therefore, close to truly ballistic conductors. Eventual high field breakdowns of these ultrashort nanotubes are also discussed.

Individual SWNT devices were fabricated by patterned CVD growth of SWNTs on SiO_2/Si wafers,⁸ followed by electron beam lithography (EBL, with a Raith 150 EBL system), metal deposition, and liftoff to form Pd source/drain (S/D) top-contacts. The lengths of SWNTs were defined by the distances between the edges of the Pd electrodes, and varied down to 10 nm (Fig. 1). The diameters of the nanotubes used for this work were all in the range of 1.5 to 2.5 nm. The heavily p-doped Si substrate was used as the back-gate with thermally grown SiO_2 as the gate dielectric. All room temperature data presented here were recorded with the samples exposed to air.

Nearly all of our Pd contacted metallic SWNTs (with weak or no gate dependence) exhibit low-bias (V_{DS}) conductance in the range of 2 to $4e^2/h$ (for $L < 1 \mu\text{m}$, also see Ref. 7) at room temperature. Upon cooling, the nanotubes with $L > 200 \text{ nm}$ always show increased conductance. In contrast, the conductance of nanotubes with $L < 100 \text{ nm}$ are largely temperature independent. Fig. 2 shows the conductance vs. gate voltage (V_{GS}) curves for a $L \sim 60 \text{ nm}$ SWNT recorded at several temperatures. The conductance is essentially independent of temperature except for the appearance of conductance oscillations below 40 K (Fig. 2). At 1.5 K, G vs. V_{GS} and V_{DS} evolves into a clear interference pattern (Fig. 2b) that corresponds to a Fabry-Perot resonator.² The temperature independence of conductance suggests that electron backscattering by acoustic phonons (twistons)⁹ is ineffective in the 60 nm long SWNT and $l_{\text{ap}}(300\text{K}) \gg 60$

nm. In the low bias regime, transport in SWNTs with $L \sim 60$ nm is ballistic and free of acoustic phonon scattering even at room temperature.

Transport properties of ohmically contacted metallic SWNTs in the low and high bias regimes have been measured at 290 K as a function of tube lengths. Under low biases, we consistently measure higher conductance for shorter tubes. Current vs. bias voltage (I_{DS} vs. V_{DS}) curves in Fig. 3 show that the low bias conductance of SWNTs for a $L \sim 55$ nm tube is $\sim 3.5 e^2/h$, higher than $\sim 2 e^2/h$ for a $L \sim 700$ nm tube. At high biases, currents saturate at the ~ 20 μA level for long tubes ($L \sim 700$ nm and 300 nm) due to optical or zone boundary phonon scattering,¹ and reaches 60 μA for a short $L \sim 55$ nm (Fig. 3). Shorter tubes ($L < 100$ nm) exhibit different slopes in the high-bias regime of the I_{DS} - V_{DS} curves than in the low-bias regime, and do not show current saturation.

To determine whether these results were consistent with the expected mean-free-paths, we performed Monte Carlo simulations of the I_{DS} - V_{DS} characteristics for metallic SWNTs of various lengths. Monte Carlo simulation solves the Boltzmann transport equation stochastically and has been used extensively for treating high-field transport in semiconductor devices.¹⁰ Carrier transport in one-dimensional metallic tubes differs from that typically encountered in semiconductors since, 1) the metallic band has a linear E-k relation without a band gap, and 2) carriers are highly degenerate, which necessitates the treatment of Pauli blocking of scattering events. The linear E-k relation results in a constant density-of-states and energy-independent scattering rate (in these initial studies, we neglected scattering to the higher, semiconductor like bands). Two scattering mechanisms were included. The first is backscattering by acoustic phonons with an assumed constant scattering rate of $1/\tau_{ap} = v_F/l_{ap}$ where v_F is the Fermi velocity. After

backscattering by an acoustic phonon, the carrier energy is conserved and velocity direction reversed. The second is backscattering by optical phonon (with small \mathbf{k} vector) and zone-boundary phonon (with large \mathbf{k} vector) emission with a scattering rate of $1/\tau_{\text{op}} = v_F/l_{\text{op}}$. Only phonon emission was treated; optical and zone-boundary phonon absorption was omitted since the phonon energies are much larger than the thermal energy at room temperature. Elastic scattering due to defects was ignored in the calculations since its mfp is $l_e \geq 1 \mu\text{m}$,⁷ greater than l_{ap} for our CVD grown materials. To treat carrier degeneracy, we used an ensemble Monte Carlo method as described by Lugli.¹¹ The position and energy-dependent distribution function was updated after each time-step so that the probability that a final state was empty could be evaluated. The contacts were assumed to be ideal (i.e. no reflection at contacts). The level of treatment was essentially that of Ref. 1 using the phonon mfps as fitting parameters without treating the detailed phonon dispersion relation (macroscopic theory), but the Monte Carlo simulation facilitates the treatment of so-called off-equilibrium transport in short tubes under high bias. It can also be readily extended to include phonon dispersion characteristics and additional scattering mechanisms.

Fitting the calculated $I_{\text{DS}}-V_{\text{DS}}$ curves to the experimental results reveals a mfp of $l_{\text{ap}} \approx 300\text{nm}$ for acoustic phonon backscattering and a mfp of $l_{\text{op}} \approx 15\text{nm}$ for optical phonon backscattering (Fig. 3). The channel conductance under low bias is controlled by l_{ap} and that under high bias is controlled by l_{op} . Notice that the calculation underestimates the measured low bias conductance for $L \sim 700\text{nm}$, so $l_{\text{ap}} \approx 300\text{nm}$ should be the lower limit of the mfp for acoustic phonon backscattering. The upper limit (which is obtained by fitting the low bias $I_{\text{DS}}-V_{\text{DS}}$ for $L \sim 700\text{nm}$ only) may be a factor of ~ 2 larger. The best

fitting results to all of the curves are obtained when a phonon energy of $\hbar \Omega \sim 0.2$ eV is used, close to the energies of optical and zone boundary phonon in the range of 1300 to 1580 cm^{-1} . Our fitting is nevertheless imperfect, which could be due to errors in the lengths of the short tubes measured by atomic force microscopy, and small variations in the quality of the tubes and contacts for the devices studied. The mfps and optical phonon energies obtained here are similar to those obtained by fitting experimental data^{1,12} (Note that Ref 12 parallels with the current work). However, the mfp of $l_{\text{op}} \approx 15$ nm is shorter than the ~ 100 nm value that has been estimated from the deformation potential.¹ Further work on the detailed phonon dispersion relations and the deformation potential is needed to understand the difference.

A simple method based on an empirical formulism of resistance can also be used to analyze the experiment $I_{\text{DS}}-V_{\text{DS}}$ curves and extract the phonon scattering mfps. Since optical phonon scattering is dominant over acoustic phonon and elastic scatterings in the high bias regime for short nanotubes, the effective mfp for electron backscattering is largely set by the l_{op} , $l_{\text{eff}}^{-1} = l_{\text{e}}^{-1} + l_{\text{ap}}^{-1} + l_{\text{op}}^{-1} \approx l_{\text{op}}^{-1}$. The slope of the nanotube I_{DS} vs. V_{DS} probed under high bias can be written as, $G = \Delta I_{\text{DS}} / \Delta V_{\text{DS}} = G_0 T$, where $G_0 = 4e^2 / h$ and $T = l_{\text{op}} / (l_{\text{op}} + L)$ is the transmission probability¹³ between the source and drain in the presence of optical phonon scattering. Fittings of the slopes for all of the $I_{\text{DS}}-V_{\text{DS}}$ curves in the high-bias regime suggest $l_{\text{op}} \sim 11$ nm, similar to $l_{\text{op}} \sim 15$ nm from Monte Carlo calculations. The results here represent the first time that the strengths of electron couplings with both acoustic and optical phonons are elucidated in a quantitative manner based on length dependent nanotube transport properties.

The short mfp l_{op} for optical phonon scattering suggests that truly ballistic transport in SWNTs under high bias requires length scaling to the nanometer scale. The shortest metallic SWNT device that we have fabricated is $\sim 10 \pm 5$ nm long between Pd electrodes (uncertainty due to the finite resolution of atomic force microscopy). Up to 70 μA current can flow through the ~ 10 nm tube at $V_{\text{DS}} \sim 2.6\text{V}$, beyond which breakdown of the nanotube is observed (Fig. 4a). On the same nanotube, a $L \sim 300$ nm long segment exhibits a current carrying limit of $I_{\text{DS}} \sim 25 \mu\text{A}$ and breakdown voltage of $V_{\text{DS}} \sim 4$ V (Fig. 4b), while a $L \sim 3 \mu\text{m}$ long segment breaks down at a much higher voltage of $V_{\text{DS}} \sim 13.8$ V and lower current of $I_{\text{DS}} \sim 18 \mu\text{A}$ (Fig. 4c). In shorter nanotubes, electrons encounter less backscattering and accelerate to high energies rapidly, and thus breakdowns occur at lower biases. For the $3 \mu\text{m}$ long nanotube, electrical breakdown most likely occurs at defect sites on SWNTs (the mfp for elastic defect elastic scattering is typically $l_e < 3 \mu\text{m}$ for CVD grown nanotubes^{5,7}).¹⁴ For the medium length $L \sim 300$ nm nanotube section, breakdown may be related to joule heating as a result of electron/optical phonon coupling and the resulting oxidation in air.¹⁵ The breakdown of the ultra short $L \sim 10$ nm SWNT segment appears different from the longer segments in that its $I_{\text{DS}}-V_{\text{DS}}$ curve exhibits only slight flattening beyond $V_{\text{DS}} \sim 0.2$ V (indicating optical phonon scattering not as effective), and shows a steeper slope beyond ~ 1.4 V prior to breakdown at ~ 2.6 V. The steeper $I_{\text{DS}}-V_{\text{DS}}$ beyond ~ 1.4 V is likely to be due to conduction through the first non-crossing higher sub-band in the metallic tube, which has a band gap of $E_g \approx 2.6(eV)/d(\text{in nm}) \approx 1.3eV$.¹⁶ The mechanism of eventual breakdown could involve high field ($\sim 10^6$ V/cm) impact ionization^{17,18} (likely assisted by residue optical phonon scattering) involving carriers in the higher subbands. It is also possible that

electro-migration occurs in the thin and small Pd electrodes and metal-tube contacts degrade under the high current density ($\sim 10^7 \text{ A/cm}^2$ in the Pd electrodes). Due to the importance of high current delivery capability of SWNT devices, we have also investigated high field transport in Pd ohmically contacted short ($L \sim 50 \text{ nm}$, slightly longer than l_{op}) semiconducting SWNTs (s-SWNT).⁵ In the p-type on-states, short s-SWNTs exhibit an upturn beyond $V_{\text{DS}} \sim 1 \text{ V}$ prior to complete breakdown at $\sim 2.2 \text{ V}$ (maximum current $\sim 70 \mu\text{A}$) (Fig. 4d). In this case, the current upturn can be attributed to injections of electrons to the conduction band¹⁹ and subsequently into higher subbands of the nanotube under the increasing bias voltage. The breakdown of semiconducting nanotubes could be due similar effects as in metallic nanotubes as described above. Detailed work is necessary to fully understand transport near the breakdown regime in quasi-ballistic nanotubes.

In summary, SWNTs with highly reproducible ohmic contacts and various lengths are investigated by electron transport experiments and theory. The mean free paths for acoustic and optical phonon scatterings are determined. Short nanotubes ($\sim 10 \text{ nm}$) are ballistic and quasi-ballistic in the low and high bias regimes respectively. Remarkably high currents up to $70 \mu\text{A}$ can flow through these short tubes. The eventual breakdowns for ballistic metallic and semiconducting nanotubes are discussed and deserve further investigation due to their importance to high power transistors or interconnects.

The authors are indebted to Prof. Supriyo Datta of Purdue University and Dr. M. P. Anantram of NASA Ames Research Center for extensive technical discussions. This work was supported by MARCO MSD Focus Center, DARPA's Moletronics program, and the NSF Network for Computational Nanotechnology.

Figure Captions

Fig 1. Atomic force microscopy (AFM) images of five devices consisting of individual SWNTs with lengths in the range of $L=600$ nm to 10 nm between the edges of Pd contact electrodes.

Fig. 2. Electrical properties of a $L \sim 60$ nm long ohmically contacted metallic SWNT (diameter ~ 1.5 nm). a) G vs. V_{GS} recorded (under a low bias of $V_{DS}=1$ mV) at 290 K, 150 K and 40 K respectively. A noteworthy technical point is that thin Pd contact electrode fingers were used (250 nm \times 25 nm) for contacts in order to form small (< 100 nm) gaps between electrodes by liftoff. The resulting narrow Pd electrodes had a resistance of ~ 0.6 k Ω at 290K and a negligibly small resistance of 0.019 k Ω at 40 K. The series resistance was estimated from the geometry of the contact electrodes and the resistivity of the Pd film at various temperatures. The data shown here was after the correction of the series resistance of the Pd electrodes. b) Differential conductance vs. V_{DS} and V_{GS} for the device recorded at 2 K. The arrow points to a resonance peak,^{2,7} at $V_{DS} = \pi \hbar v_F / eL = 25$ mV where $v_F = 8.1 \times 10^5$ m/s is the Fermi's velocity and $L \sim 60$ nm. The gate oxide thickness $t_{ox} \sim 10$ nm for the device in this figure.

Fig. 3. Electrical properties of ohmically contacted metallic SWNTs of various lengths (diameters $d \sim 2$ - 2.5 nm, oxide thickness $t_{ox} \sim 10$ nm for the samples in this figure). Solid lines are experimental I_{DS} - V_{DS} curves and the symbols are Monte Carlo calculation and fitting results. Note that the devices in Fig. 3 had a series resistance of ~ 1 k Ω arising from the thin Pd electrodes except for the 55 nm long tube which had an electrode

resistance of $\sim 3 \text{ k}\Omega$. The experimental curves are all after correction of V_{DS} . We also note that for short tubes ($< 100 \text{ nm}$), a permanent change in the electrical properties was observed after applying large fields ($V_{DS} > 1 \text{ V}$). This could be due to the degradation of the contacts at such high drain biases, and requires further work to illuminate the exact cause.

Fig. 4. I_{DS} - V_{DS} breakdown characteristics of SWNTs. The lengths of three sections of a metallic SWNT are a) $\sim 10 \text{ nm}$, b) $\sim 300 \text{ nm}$ and c) $\sim 3 \text{ }\mu\text{m}$, with the Si substrate being grounded. The gate oxide thickness $t_{ox} \sim 67 \text{ nm}$ for the samples. d) I_{DS} - V_{DS} data recorded for a semiconducting SWNT (in the ON state under $V_{GS}=0\text{V}$) with $L \sim 50 \text{ nm}$ and $t_{ox} \sim 10 \text{ nm}$ (inset shows I_{DS} vs. V_{GS} under $V_{DS}=10 \text{ mV}$). AFM image insets in a)-c) show the devices after electrical breakdown, and arrows in b) and c) point to the breakdown points. The parasitic electrode resistance is high ($\sim 15 \text{ k}\Omega$, due to the very thin and narrow electrode geometry) for devices in a)-c). For this reason, they were not used for the quantitative analysis of I_{op} in Fig. 3.

References and Notes

- ¹ Z. Yao, C. L. Kane, and C. Dekker, Phys. Rev. Lett. **84**, 2941 (2000).
- ² W. Liang, M. Bockrath, D. Bozovic, et al., Nature **411**, 665 (2001).
- ³ J. Kong, E. Yenilmez, T. W. Tombler, et al., Phys. Rev. Lett. **87**, 106801 (2001).
- ⁴ A. Javey, H. Kim, M. Brink, et al., Nature Materials **1**, 241 (2002).
- ⁵ A. Javey, J. Guo, Q. Wang, et al., Nature **424**, 654 (2003).
- ⁶ P. L. McEuen, M. S. Fuhrer, and H. K. Park, IEEE Trans. Nanotechnology **1**, 78 (2003).
- ⁷ D. Mann, A. Javey, J. Kong, et al., Nano Lett. **3**, 1541 (2003).
- ⁸ J. Kong, H. Soh, A. Cassell, et al., Nature **395**, 878 (1998).
- ⁹ C. L. Kane, E. J. Mele, R. Lee, et al., Euro. Phys. Lett. **6**, 683 (1998).
- ¹⁰ M. Lundstrom, *Fundamentals of carrier transport, 2nd edition* (Cambridge University Press, 2000).
- ¹¹ P. Lugli and D. K. Ferry, IEEE Trans. Elec. Dev. **32**, 2431 (1985).
- ¹² J.-Y. Park, S. Rosenblatt, Y. Yaish, et al., cond-mat/0309641.
- ¹³ S. Datta, *Electronic Transport in Mesoscopic Systems* (University Press, Cambridge, 1995).
- ¹⁴ A large gap was observed in the 3 μm long nanotube after breakdown, likely due to electron field emission and arcing in air during breakdown caused by high local fields at the break points. The nanotube section near the break points became wavy (was straight before), indicating mechanical ‘jolt’ during the breakdown.
- ¹⁵ P. G. Collins, M. Hersam, M. Arnold, et al., Phys. Rev. Lett. **86**, 3128 (2001).
- ¹⁶ M. P. Anantram, Phys. Rev. B **62**, R4837 (2000).

- ¹⁷ S. M. Sze, *Physics of semiconductor devices* (Wiley, New York, 1981).
- ¹⁸ N. Sano and A. Yoshii, Phys. Rev. B **45**, 454171 (1992).
- ¹⁹ M. Radosavljevic, S. Heinze, J. Tersoff, et al., Appl. Phys. Lett. **83**, 2435 (2003).

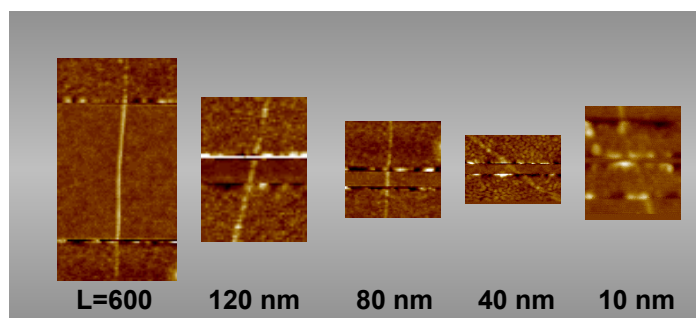


Figure 1

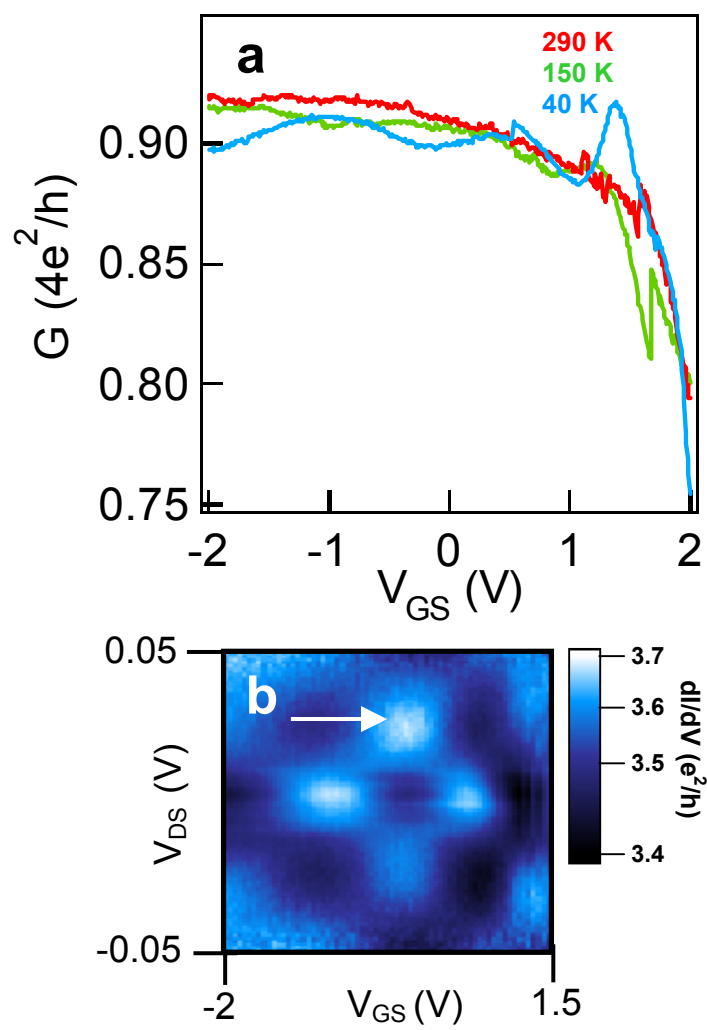
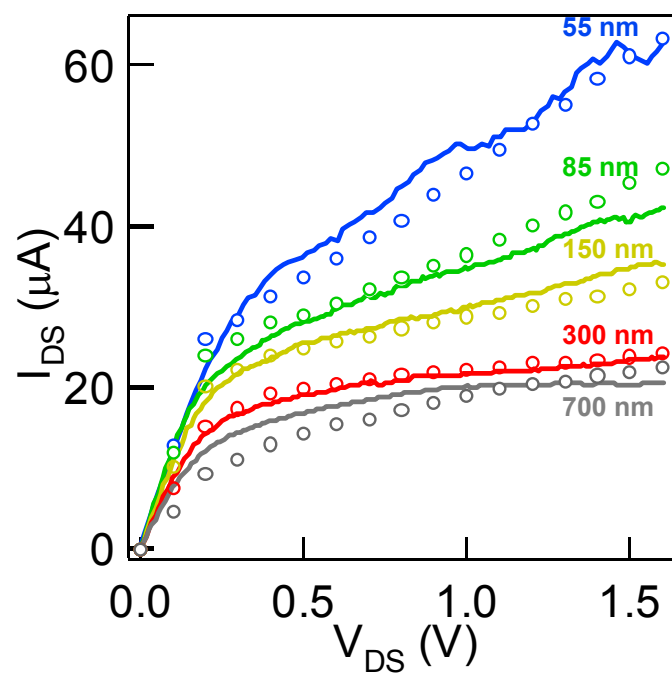


Figure 2

**Figure 3**

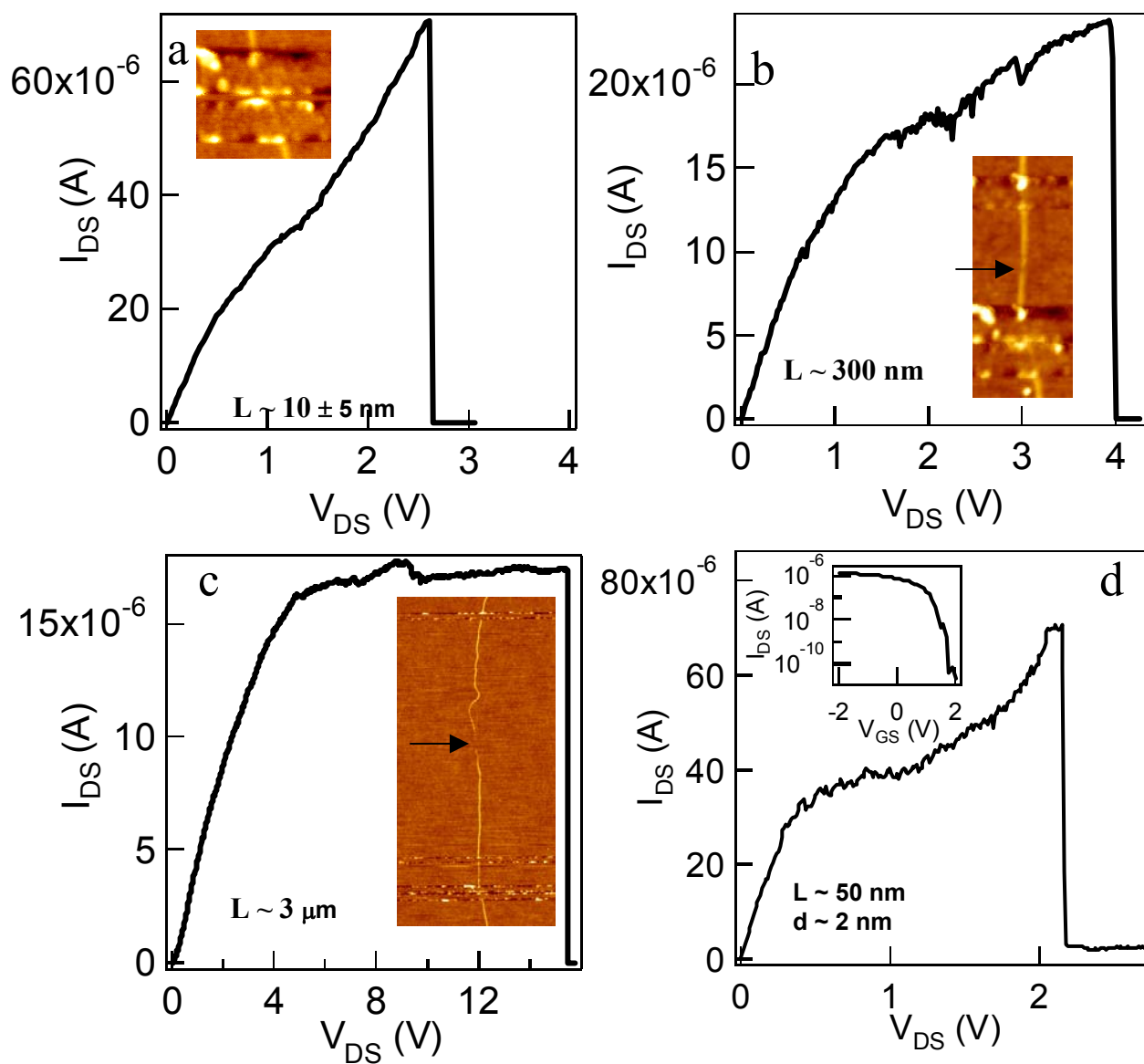


Figure 4